The High-Resolution Structure of 3-Deoxy-D-*arabino*-heptulosonate-7-phosphate Synthase Reveals a Twist in the Plane of Bound Phosphoenolpyruvate[†,‡]

Igor A. Shumilin, Ronald Bauerle, and Robert H. Kretsinger*

Department of Biology, University of Virginia, Charlottesville, Virginia 22903

Received November 27, 2002; Revised Manuscript Received February 7, 2003

ABSTRACT: 3-Deoxy-D-*arabino*-heptulosonate-7-phosphate synthase (DAHPS), the first enzyme of the aromatic biosynthetic pathway in microorganisms and plants, catalyzes the aldol-like condensation of phosphoenolpyruvate (PEP) and D-erythrose 4-phosphate (E4P) with the formation of DAHP. The native and the selenomethionine-substituted forms of the phenylalanine-regulated isozyme [DAHPS(Phe)] from *Escherichia coli* were crystallized in complex with PEP and a metal cofactor, Mn^{2+}, but the crystals displayed disorder in their unit cells, preventing satisfactory refinement. However, the crystal structure of the E24Q mutant form of DAHPS(Phe) in complex with PEP and Mn^{2+} has been determined at 1.75 Å resolution. Unlike the tetrameric wild-type enzyme, the E24Q enzyme is dimeric in solution, as a result of the mutational perturbation of four intersubunit salt bridges that are critical for tetramer formation. The protein chain conformation and subunit arrangement in the crystals of E24Q and wild-type DAHPS are very similar. However, the interaction of Mn^{2+} and PEP in the enzymatically active E24Q mutant complex differs from the Pb^{2+}−PEP and Mn^{2+}−phosphoglycolate interactions in two enzymatically inactive wild-type complexes whose structures have been determined previously. The geometry of PEP bound in the active site of the E24Q enzyme deviates from planarity due to a 30° twist of the carboxylate plane relative to the enol plane. In addition, seven water molecules are within contact distance of PEP, two of which are close enough to its C2 atom to serve as the nucleophile required in the reaction.

The first step of the common pathway leading to the biosynthesis of most aromatic compounds in microorganisms and plants is the aldol-like condensation of phosphoenolpyruvate (PEP)[1] and D-erythrose 4-phosphate (E4P), forming 3-deoxy-D-*arabino*-heptulosonate 7-phosphate (DAHP) with the release of the phosphate of PEP. The reaction is catalyzed by the metal-activated enzyme, DAHP synthase (DAHPS) (*1*), which in most microorganisms is the target for pathway regulation by negative feedback inhibition. In *Escherichia coli*, there are three DAHPS isozymes, each specifically regulated by one of the three aromatic amino acid end products, either Phe, Tyr, or Trp.

We have recently determined the crystal structures of three forms of the Phe-regulated isozyme of *E. coli*: DAHPS-(Phe) in complex with PEP and Pb^{2+}, a poorly activating metal (*2*); DAHPS(Phe) in complex with the nonutilizable PEP analogue 2-phosphoglycolate (PGL) and Mn^{2+}, the most efficient metal activator (*3*); and DAHPS(Phe) in complex with PEP, Mn^{2+}, and Phe, the feedback inhibitor (*4*). These studies have established the overall fold of the enzyme and many details of the structure of its catalytic and regulatory sites.

The DAHPS(Phe) monomer is a $(\beta/\alpha)_8$ barrel enhanced with an N-terminal extension (strand β0 followed by helices α00 and α0) and an extra β6a/β6b sheet inserted before the β6 strand of the barrel (*2*). Enzyme monomers form tight dimers that in turn associate into tetramers with 222 symmetry, held together by a limited number of interactions between interface residues. The active site of the enzyme is made up of residues from a single monomer and is located in a cleft at the C-end of the barrel. The coordination of PEP and metal in the active site is well-defined; however, the binding site for E4P is presently only inferred from its fortuitous occupancy by a SO_4^{2-} ion present in the crystallization solution. The feedback site of DAHPS(Phe) is composed of residues from both monomers of a tight dimer and is located ∼20 Å from the nearest active site (*4*). The mechanism of allosteric regulation involves two interrelated paths of conformational changes, one propagated within the enzyme monomer and the other between the subunits of the tight dimer. Together, these transmit the inhibitory signal

[†] This research was supported by Grants MCB-0110877 (R.H.K.) and MCB-0110984 (R.B.) from the National Science Foundation and Grant J-563 from the Jeffress Memorial Trust.

[‡] The coordinates of the refined structure have been deposited with the Protein Data Bank (entry 1N8F).

* To whom correspondence should be addressed: Department of Biology, University of Virginia, Gilmer Hall, Charlottesville, VA 22903-2477. Phone: (434) 982-5764. Fax: (434) 982-5626. E-mail: rhk5i@virginia.edu.

[1] Abbreviations: PEP, phosphoenolpyruvate; E4P, D-erythrose 4-phosphate; DAHP, 3-deoxy-D-*arabino*-heptulosonate 7-phosphate; PGL, 2-phosphoglycolate; DAHPS, 3-deoxy-D-*arabino*-heptulosonate-7-phosphate synthase; DAHPS(Phe), Phe-regulated DAHPS; KDOPS, 2-keto-D-*manno*-2-octulosonate-8-phosphate synthase; *A.a.* KDOPS, KDOPS from *Aquiflex aeolicus*; A5P, D-arabinose 5-phosphate; EPSPS, 5-enolpyruvylshikimate-3-phosphate synthase; S3P, shikimate 3-phosphate; GPJ, glyphosate; BTP, 1,3-bis[tris(hydroxymethyl)methylamino]-propane; EDTA, ethylenediaminetetraacetic acid; MR, molecular replacement; MAD, multiwavelength anomalous dispersion; NCS, noncrystallographic symmetry; rmsd, root-mean-square deviation.

10.1021/bi027257p CCC: $25.00
Published on Web 03/12/2003

Table 1: Data Collection and Refinement Statistics for DAHPS−Mn−PEP Crystals

	E24Q	wild type 1	wild type 2	SeMet
diffraction data				
*C*2 unit cell	213.2 Å, 53.3 Å, 150.2 Å, 116.9°	209.9 Å, 53.1 Å, 150.2 Å, 115.7°	210.2 Å, 53.1 Å, 150.3 Å, 115.6°	211.8 Å, 53.3 Å, 151.2 Å, 116.4°
resolution (Å)	20.0−1.75	20.0−2.15	20.0−2.3	20.0−2.5
no. of unique reflections	151346	76652	64383	48308
completeness[a] (%)	99.4 (98.6)	93.8 (80.6)	95.9 (76.8)	91.4 (74.3)
multiplicity[a]	4.2 (3.8)	4.3 (3.8)	5.8 (3.2)	5.5 (3.7)
$\langle I\rangle/\langle\sigma(I)\rangle$[a]	15.5 (2.5)	23.9 (8.6)	22.3 (6.3)	14.7 (3.0)
R_{merge}[a] (%)	5.9 (34.8)	5.3 (11.9)	6.8 (13.9)	7.5 (27.1)
outermost shell (Å)	1.81−1.75	2.23−2.15	2.38−2.3	2.59−2.5
refinement				
rmsd for bond lengths (Å)	0.006	0.008	0.008	0.006
rmsd for bond angles (deg)	1.2	1.3	1.3	1.2
average *B*-factor (protein) (Å^2)	31.3	42.5	50.8	48.6
R_{work}/R_{free} (%)	20.9/23.7	25.1/29.6	26.6/30.2	23.1/26.5
test set (%)	2.0	2.6	2.9	2.7

[a] Values in parentheses are for the outermost resolution shell.

from the Phe binding site to the active site, preventing the binding of E4P and flipping the orientation of bound PEP. A similar understanding of the catalytic mechanism of DAHPS has still not been achieved in part because all of the determined crystal structures are of enzyme complexes that lack catalytic activity.

Here we report the results of crystallographic studies of two enzymatically active DAHPS forms, the wild-type DAHPS(Phe)−Mn−PEP complex and the mutant E24Q DAHPS−Mn−PEP complex. The E24Q mutation alters four electrostatic interactions that are crucial for tetramer formation (*2*), thereby rendering the enzyme a dimer in solution (manuscript in preparation). Unfortunately, refinement of the wild-type crystal structure was confounded by apparent disorder in the unit cell. However, the crystal structure of the E24Q enzyme, which has kinetic properties similar to those of the wild-type enzyme, has been determined and refined to 1.75 Å. The structure reveals that the plane of PEP bound at the active site is twisted 30° about its C−C single bond. This structural distortion of PEP is very likely a crucial step in the reaction mechanism of the enzyme.

MATERIALS AND METHODS

Protein Purification and Crystallization. The E24Q, E24A, R124A, and H217A replacements were introduced by site-directed mutagenesis of the wild-type *aroG* gene using the Promega Altered Sites procedure (manuscript in preparation). The E24Q enzyme was purified by dye ligand chromatography on Dyematrex gel Blue A (Amicon Corp.) following the general protocol developed for the wild-type enzyme (*5*). The E24A, R124A, and H217A enzymes were purified similarly except that Mono Q ion exchange FPLC chromatography was used instead of dye ligand chromatography. The native and SeMet-substituted wild-type enzymes were purified as previously described (*4*, *5*). The purified enzymes were made metal-free by exhaustive dialysis against 10 mM EDTA in 5 mM 1,3-bis[tris(hydroxymethyl)methylamino]-propane (BTP) buffer (pH 7.0) and then against 1.0 mM BTP buffer (pH 7.0) to remove EDTA.

All solutions used for crystallization, except for the solutions of $MnSO_4$ and protein, were treated with Chelex 100 to remove metal cations. The crystals were grown at room temperature in 8−10 μL hanging drops using the vapor diffusion method. Wild-type and SeMet-substituted DAHPS−Mn−PEP crystals grew in the drops with 7 mg/mL protein, 4.2 mM PEP, 0.7 mM $MnSO_4$, 0.1 M Li_2SO_4, and 12% (w/v) PEG1000 in 50 mM BTP (pH 8.7). The reservoir solution contained 19% PEG1000, 0.1 M Li_2SO_4, and 20% (v/v) ethanol in 50 mM BTP (pH 8.7). The best diffracting crystals of the E24Q DAHPS−Mn−PEP complex were grown in a drop containing 7 mg/mL E24Q DAHPS, 4.2 mM PEP, 0.7 mM $MnSO_4$, 0.1 M Li_2SO_4, and 12% (w/v) PEG4000 in 50 mM BTP (pH 8.1). The reservoir solution contained 30% PEG4000, 0.1 M Li_2SO_4, and 20% (v/v) ethanol in 50 mM BTP (pH 8.1). The crystals of the E24A and R124A DAHPS−Mn−PEP complexes grew under the same conditions but had a platelike shape and lower diffraction limits. Variations in pH and in the concentration of the components and the use of different PEGs and salt additives did not significantly improve the quality of these crystals.

Data Collection and Refinement. All data sets were collected at beamline X4A at the NSLS from single crystals flash-frozen in an evaporating nitrogen stream. The data from the wild-type DAHPS−Mn−PEP crystal were collected first (Table 1). The crystal belonged to space group *C*2 and diffracted to 2.15 Å with the following cell dimensions: $a = 209.9$ Å, $b = 53.1$ Å, $c = 150.2$ Å, and $\beta = 115.7°$. There is one tetramer of DAHPS in the asymmetric unit; the water content of the crystal is ~52%. Data were processed with HKL2000 (*6*) and programs of the CCP4 suite (*7*). A molecular replacement (MR) search performed using CNS (*8*) with the enzyme subunit from the DAHPS−Mn−PGL structure as a model located all four subunits in the asymmetric unit. The structure was adjusted with O (*9*) and refined with CNS, REFMAC (*7*), and ARP (*10*). However, the R and R_{free} values did not improve after reaching 25.1 and 29.6%, respectively, despite multiple rounds of manual adjustment and refinement. The quality of the electron density varied significantly in the DAHPS tetramer. The best density was found in the residues of subunit B and regions of subunits A, C, and D located near subunit B, while more distant regions of subunits A, C, and D had multiple undefined side chains and breaks in the density.

Since the problem with the refinement of the wild-type DAHPS−Mn−PEP structure could potentially be related to some error in the data, a second set of data was collected

from another wild-type DAHPS−Mn−PEP crystal grown in a different batch (Table 1). This crystal had nearly identical cell dimensions (a = 210.2 Å, b = 53.1 Å, c = 150.3 Å, and β = 115.6°) and diffracted to 2.3 Å. However, the refinement encountered similar problems as before. The R and R_{free} values stabilized at 26.6 and 30.2%, respectively, and the regions of the tetramer distant from subunit B had the worst electron density.

Two data sets near the Se K absorption edge were measured from a SeMet-substituted DAHPS−Mn−PEP crystal (Table 1). This crystal also belonged to space group *C*2 and diffracted to 2.5 Å with the following cell dimensions: a = 211.8 Å, b = 53.3 Å, c = 151.2 Å, and β = 116.4°. The data were processed and scaled with HKL2000 and programs of the CCP4 suite. The MR search was carried out with CNS using the enzyme subunit with Met residues replaced with Ala as a model. All four subunits in the asymmetric unit were identified, and the positions of 28 Se atoms were established from the difference Fourier map and used for MAD phasing with MLPHARE and DM (*7*). Experimental phases were combined with phases calculated from the model in the refinement. O was used for structure adjustment, and CNS and REFMAC were used for refinement. After R and R_{free} reached 23.1 and 26.5%, respectively, model adjustment and further refinement did not improve the residual values. Many side chains on the outside of a molecule had poorly defined electron density, and the quality of the density varied in the tetramer as it did in the wild-type crystals.

Finally, 1.75 Å resolution data were collected from an E24Q DAHPS−Mn−PEP crystal (Table 1). This crystal also belonged to space group *C*2 with the following cell dimensions: a = 213.2 Å, b = 53.3 Å, c = 150.2 Å, and β = 116.9°. The MR solution was refined using ARP and CNS without symmetry restraints. The electron density was well-defined throughout the tetramer located in the asymmetric unit. A search for the bound water molecules was carried out with ARP. All waters that were related by the noncrystallographic symmetry operators to two or three symmetry mates were retained. Waters that had only one or no symmetry mates were inspected on the basis of their temperature factors and suitable positions for hydrogen bonding. The R and R_{free} values are 20.9 and 23.7%, respectively, for the final model that includes 10 424 protein atoms, four Mn^{2+} and PEP molecules, eight sulfates, and 1395 water molecules. Alternative conformations were observed for several side chains. The model has good stereochemistry as analyzed by PROCHECK (*11*) with 91.6% of the residues in the most favored regions of the Ramachandran plot. The coordinates and structure factors have been deposited in the Protein Data Bank as entry 1N8F.

Crystals of the E24A and R124A DAHPS−Mn−PEP complexes diffracted to less than 2.3 Å resolution and were not used for data collection. They also belong to space group *C*2 and have cell dimensions similar to those described above.

RESULTS

Attempts To Refine the Wild-Type DAHPS−Mn−PEP Structure. The wild-type DAHPS(Phe)−Mn−PEP complex crystallizes under the same conditions as do the previously determined DAHPS−Pb−PEP and DAHPS−Mn−PGL structures. All of these crystals belong to space group *C*2 with very similar unit cell dimensions, and all have a tetramer in the asymmetric unit. However, while DAHPS−Pb−PEP and DAHPS−Mn−PGL complexes were successfully refined with good R and R_{free} values and stereochemistry (*2*, *3*), all attempts to refine the structure of the DAHPS−Mn−PEP complex were problematic. These included the analysis of two independent data sets measured from native wild-type DAHPS−Mn−PEP crystals and a two-wavelength MAD data set from the SeMet-substituted DAHPS−Mn−PEP complex. Twinning of the crystals does not seem to contribute to the problem according to the available twinning tests.

A molecular replacement (MR) search with a DAHPS monomer as the model yielded the positions of all four subunits present in the asymmetric unit with each of the three data sets. As expected from the similarity of the unit cells, these positions are very similar to positions of subunits in the DAHPS−Pb−PEP and DAHPS−Mn−PGL crystals. However, none of three independent attempts to refine the DAHPS−Mn−PEP structure yielded satisfactory agreement factors or well-defined electron density maps. In all cases, the residues of subunit B and the regions of the other subunits bordering it have the lowest temperature factors and exhibit clear electron density (Figure 1a). The temperature factors of subunits A, C, and D are significantly higher (Table 2), and the σ levels of their electron densities are lower, especially at the surface regions where many side chains are undefined in the density (Figure 1b). The poorest quality electron density is observed at the surface of subunit C that is most distant from subunit B.

In all structures of the DAHPS complexes, subunit B forms the most extensive contacts with the neighbor tetramers in the crystal, while the areas of the other three subunits involved in these interactions are significantly smaller (Table 2). The areas of intersubunit contact vary in the different complexes. This is caused by the small differences in the orientation of the tetramer in the unit cells due primarily to the rotation around the noncrystallographic symmetry (NCS) axis directed along the crystallographic *a* axis. As a result, the crystals of these DAHPS complexes are not isomorphous. We suggest that the poor electron density and high temperature factors observed for the DAHPS−Mn−PEP crystals are due to the distribution of the enzyme tetramer between two or more alternative orientations, probably due to the slight rotations of the entire tetramer about subunit B as a pivot. The relative occupancies of these alternative orientations of subunits are sensitive to small variations in the crystallization conditions.

Crystallographic Analysis of Mutant Enzymes with Altered Quaternary Structure. Since the problem with the refinement of the wild-type DAHPS−Mn−PEP structure appeared to be related to crystal packing, we decided to explore factors that might influence packing. We were not able to find alternative crystallization conditions for the wild-type enzyme; hence, we turned to crystallography of mutant DAHPS enzymes with single amino acid substitutions at the dimer−dimer interface that convert the quaternary structure of the enzyme in solution from tetrameric to dimeric (manuscript in preparation). The dissociative effect of these mutations is consistent with the fact that association of the tight dimers

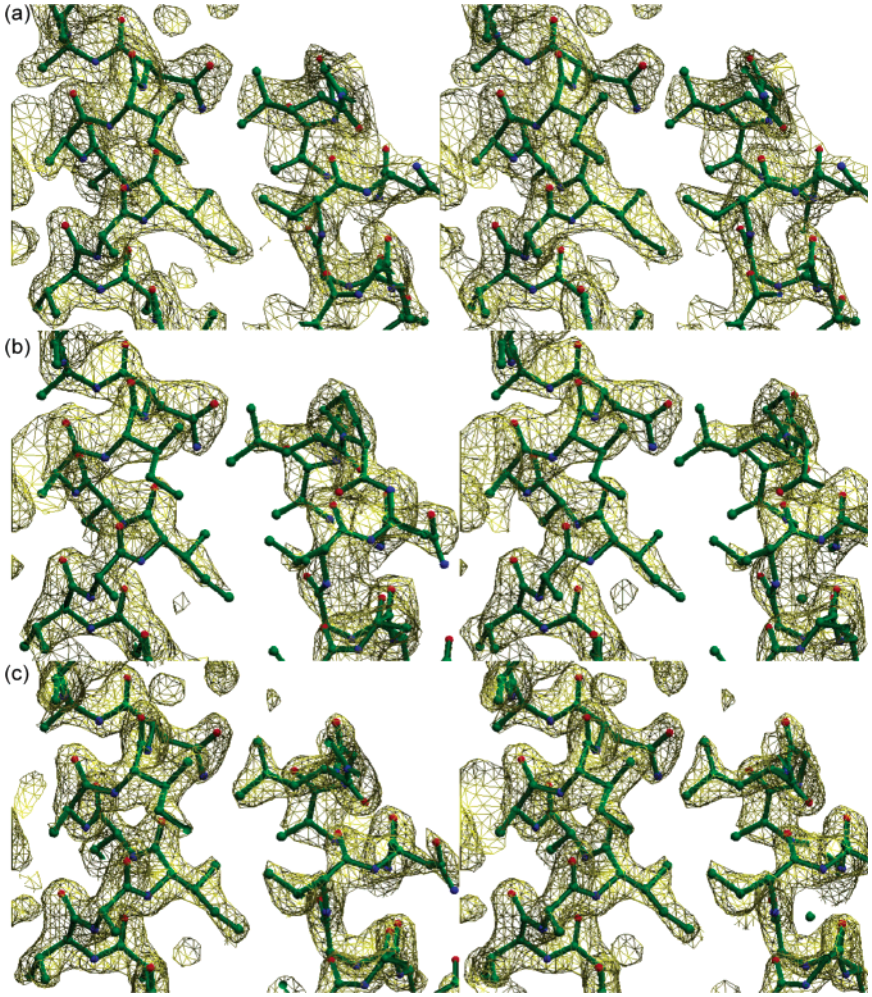

FIGURE 1: Representative electron density of wild-type (2.15 Å, R and R_{free} = 25.1 and 29.6%, respectively) and E24Q (1.75 Å, R and R_{free} = 20.9 and 23.7%, respectively) DAHPS−Mn−PEP crystals. The $2F_o - F_c$ maps are contoured at 1.3σ. (a) Subunit B of the wild-type complex has well-defined density. (b) Densities of a number of side chains in the outer regions of subunit C of the wild-type complex are poorly defined and are not improved by refinement. (c) The E24Q DAHPS−Mn−PEP complex has a well-defined density throughout the tetramer; subunit C is shown. All figures were drawn with RIBBONS (*30*).

Table 2: Surface Areas of Subunits of DAHPS Complexes Involved in Contacts with Crystallographic Mates and Average Temperature Factors

	DAHPS−Mn−PEP	SeMet DAHPS−Mn−PEP	E24Q DAHPS−Mn−PEP	DAHPS−Mn−PGL
A [area/*B*-factor (Å^2)]	500/47.8	465/60.3	493/31.1	515/37.7
B [area/*B*-factor (Å^2)]	1555/28.5	1607/32.3	1610/21.1	1392/22.3
C [area/*B*-factor (Å^2)]	470/51.7	447/62.1	523/36.0	433/42.2
D [area/*B*-factor (Å^2)]	764/42.1	778/49.0	823/31.6	620/32.7

is mediated by relatively few surface interactions (*2*). Less than 4% of the solvent accessible area of a DAHPS(Phe) subunit (550 Å^2) participates in the interdimer contact. Polar interactions between the residues of tight dimers are limited to salt bridges between the side chains of E24 and R124, H-bonds between the main chain O of E24 and Nζ of K25, and H-bonds and stacking interactions between the imidazole rings of H217 (Figure 2). The other two DAHPS isozymes in *E. coli*, i.e., DAHPS(Tyr) and DAHPS(Trp), are dimers in solution. In both of these, all four of these interacting residues are nonconserved, precluding a similar association of tight dimers into tetramers.

Site-directed substitutions E24Q, E24A, and R124A in DAHPS(Phe) have yielded enzymes that are dimeric in solution but that also retain robust catalytic activity. The V_{max} of each of the three enzymes is 60−70% of that of the wild-type DAHPS(Phe) (manuscript in preparation), similar to the activities of the naturally occurring dimeric DAHPS(Trp) and DAHPS(Tyr) isozymes (*12*). Also, the $S_{0.5}^{E4P}$ constants of these three mutant enzymes vary by no more than ±50% from the wild-type value. No tetrameric species can be detected in the purified enzymes when analyzed by either size exclusion FPLC or analytical ultracentrifugation at protein concentrations of up to 1.0 mg/mL. In contrast, the H217A enzyme displays a concentration-dependent equilibrium between the dimer and tetramer under the same conditions.

Accordingly, the E24Q, E24A, and R124A enzymes were crystallized in the presence of Mn^{2+} and PEP. Crystallization conditions were similar for the three mutant proteins but differed from those used for the wild-type complex. A lower pH, 8.1 instead of 8.7 (the calculated pI of DAHPS is ~6.6), and 30% PEG4000 instead of 19% PEG1000 as a precipitant were used. The three mutant proteins crystallize in the same

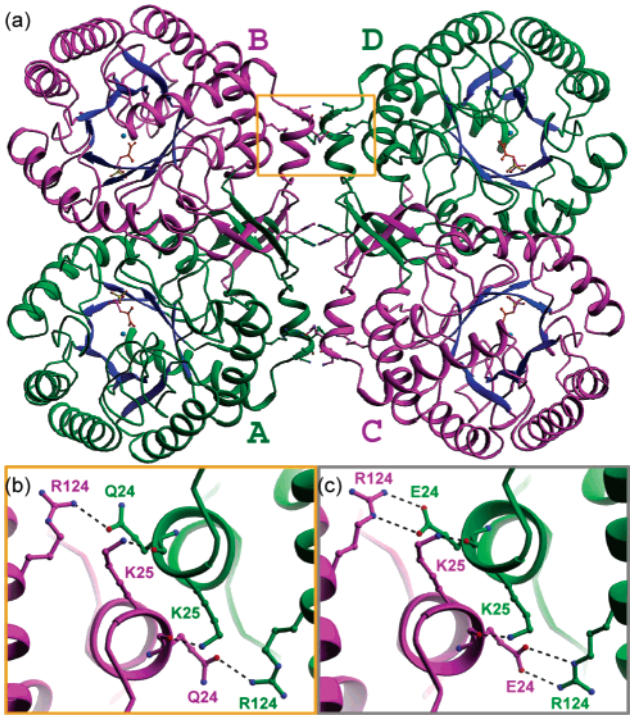

FIGURE 2: Interactions between tight dimers in the asymmetric unit of the E24Q DAHPS−Mn−PEP crystal. (a) The organization of the tetramer of E24Q in the asymmetric unit is nearly identical to that of the wild-type enzyme. E24Q consists of two tight dimers (AB and CD), each of which consists of a green and a purple subunit. The eight strands of the $(\beta/\alpha)_8$ barrel are blue in all subunits. Mn^{2+} (cyan), PEP (gold), and sulfate (yellow) are at the C-ends of the barrels. The side chains indicated along the dimer−dimer interface provide polar interactions between tight dimers. The cluster of four H217 residues is in the center, and Q24, K25, and R124 are outlined by the orange square and shown in panel b. (b) Interactions of Q24 with K25 and R124 of the neighboring subunit of the other tight dimer in the E24Q DAHPS tetramer. H-Bonds are shown as black dashed lines. (c) Interactions of E24 with K25 and R124 in the wild-type enzyme.

space group, *C*2, with unit cell dimensions very similar to those of the wild-type protein. Crystals of the E24Q enzyme have a compact shape and diffract to 1.75 Å, while both the E24A and R124A enzymes form thin platelike crystals that diffract to no better than 2.3 Å. The E24Q crystals were selected for further study, and the structure of this complex was determined by molecular replacement. The refined model has good stereochemistry and R and R_{free} values of 20.9 and 23.7%, respectively (Table 1). The electron density is well-defined throughout the molecule and shows fine details of the protein structure at high resolution (Figure 1c).

Overall Structure of the E24Q DAHPS−Mn−PEP Complex. The structure of the E24Q enzyme (hereafter termed E24Q) is similar to the structure of the wild-type DAHPS−Pb−PEP and DAHPS−Mn−PGL enzymes described previously (*2*, *3*). Although E24Q is a dimer in solution, albeit at concentrations significantly lower than those used for crystallization, the asymmetric unit of its crystal contains a tetramer, comprised of two tight dimers with 222 noncrystallographic symmetry, closely resembling the wild-type enzyme (Figure 2a). Superposition of main chain atoms of all four subunits of E24Q with those of the DAHPS−Mn−PGL complex yields an rmsd of 0.50 Å.

The orientation of the tetramer in the asymmetric unit of E24Q differs slightly from that of the wild-type enzyme. The difference is caused mostly by the rotation of the entire tetramer ~2° about an NCS axis near the crystallographic *a* axis. The altered packing is probably responsible for the greater order of the protein in the mutant crystals. Interdimer contacts in E24Q correspond to those in the wild-type enzyme. All nonpolar dimer−dimer interactions, which constitute a majority of these contacts, are retained. The cluster of four H217 residues that surround the origin of the 222 NCS in the wild-type enzyme (*2*) is also present in E24Q. This cluster is supported by the π-stacking interaction between the imidazole rings of the H217 residues of subunits A and D, and B and C, and by the interaction between Nϵ2 of the H217 residues of subunits A and C, and B and D. Pairs of Nϵ2 atoms do not form a direct H-bond as was reported previously (*2*) but are bound through H-bonds with water molecules visible at the higher resolution. H-Bonds between Nζ of K25 and the peptide O of E24 are also seen. The only difference observed in the dimer−dimer interaction is a change in the bonding between residues 24 and 124. In E24Q, there is a single H-bond between Oϵ1 of Q24 and Nη1 of R124 (Figure 2b), whereas in the wild-type DAHPS, both carboxylate O atoms of E24 participate in the H-bonds with R124, interacting with Nζ and Nη2 (Figure 2c). Thus, the loss of energy due to the change in the E24−R124 bridge is sufficient to cause the dissociation of the E24Q tetramer into dimers in solution. However, in the crystal, this energy loss is apparently compensated by the energy of the crystal contacts, resulting in the formation of a tetramer. Similar unit cell parameters were also found in the E24A and R124A crystals, where no interaction is possible between residues 24 and 124, suggesting that crystal contacts are able to compensate for an even greater energy loss.

The two tight dimers located in the asymmetric unit of E24Q are very similar to each other (rmsd of 0.29 Å for main chain atoms) and to the respective tight dimers of the wild-type protein (rmsd of 0.30 Å). The numerous polar and nonpolar contacts between subunits comprising the tight dimer are unaffected by the E24Q substitution, which is located away from the intersubunit interface. These contacts include interactions between residues of a three-stranded antiparallel intersubunit β-sheet (β0*−β6a−β6b),[2] of the α4 and α5 helices, and of the β2−α2, β3−α3, β4−α4, α4−β5, β5−α5, and α5−β6a loops. The total contact area is ~2750 Å^2 per subunit.

The four subunits of the asymmetric unit of E24Q are also similar to each other as well as to the subunits of the wild-type enzyme. The rmsd values for superposition of main chain atoms are 0.25 and 0.32 Å, respectively. As in the wild-type complex, the first seven residues at the N-terminus are disordered and not visible in the electron density maps of E24Q. These N-terminal residues become ordered upon the binding of the feedback inhibitor, L-phenylalanine, forming part of the inhibitor-binding pocket (*4*). A segment of the β8−α8 loop (residues 313−317) is disordered in the wild-type DAHPS−Pb−PEP and DAHPS−Mn−PGL structures except when stabilized by crystallographic contacts (*3*). This segment is visible in all four subunits of the E24Q DAHPS−Mn−PEP complex. However, the relatively high temperature factors of its residues, some fragmentation of the electron density, and the conformational variability

[2] Strand β0* is from the other subunit of the tight dimer.

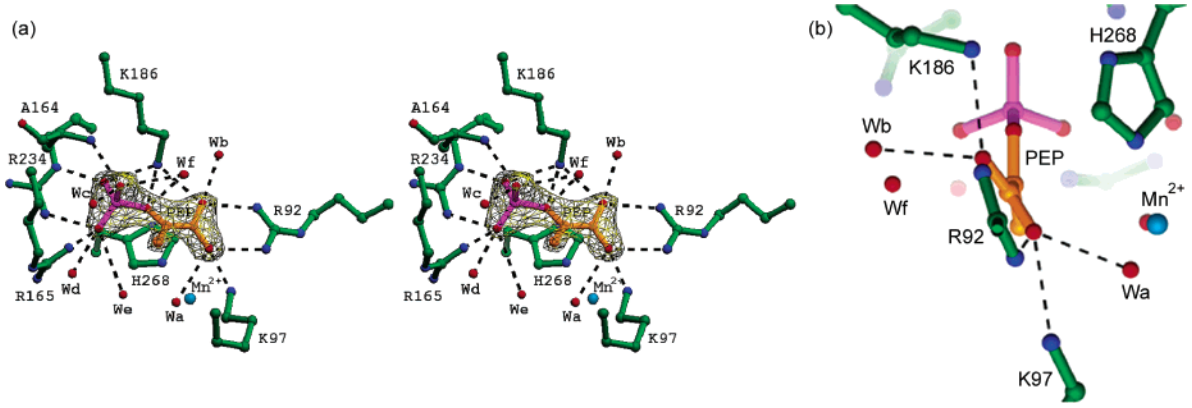

FIGURE 3: PEP binding in the active site of the E24Q DAHPS−Mn−PEP complex. (a) Stereoview of the PEP-binding site. PEP-coordinating interactions (Table 3) are shown as black dashed lines. The $F_o - F_c$ electron density map was calculated with PEP omitted from the F_c terms and is contoured at 5σ. (b) Only the interactions of the carboxylate group of PEP are shown. These interactions cause a 30° twist of the carboxylate plane relative to the enol plane, while the phosphate is tightly anchored. A charge interaction between a carboxylate O of PEP and Mn^{2+} is likely to contribute to the twist, but the distance of 3.2 Å is too long to consider this O as a ligand of Mn^{2+}. Water molecules Wa and Wf are potential candidates for an attack at C2 of PEP in the enzymatic reaction.

between subunits indicate a similar flexibility of this loop. Small differences in the conformations of several side chains in the E24Q DAHPS−Mn−PEP complex likely reflect the higher resolution of the E24Q structure (1.75 Å) and not real differences relative to the wild-type structures (2.6 and 2.0 Å). Approximately 1400 water molecules, most of which honor the NCS symmetry, are visible in the E24Q DAHPS−Mn−PEP structure compared to approximately 800 waters observed in the DAHPS−Mn−PGL structure and four waters assigned in the DAHPS−Pb−PEP structure.

Details of the Active Site and the PEP Twist in the E24Q Enzyme. As in the wild-type enzyme, the active site of E24Q is located at the C-end of the $(\beta/\alpha)_8$ barrel and is fully occupied by metal cofactor, PEP, and sulfate; the latter is inferred to occupy the position of the phosphate of E4P. The active sites of all four subunits in the asymmetric unit of the E24Q DAHPS−Mn−PEP complex are nearly identical, and both the protein ligands and the bound molecules are clearly visible in the electron density map.

Mn^{2+} is coordinated by Sγ of C61 (distance of 2.6 Å), Nϵ2 of H268 (2.2 Å), Oϵ2 of D302 (2.1 Å), and Oδ2 of E326 (2.2 Å) and by the water molecule Wa H-bonded to K97 (2.2 Å). A carboxylate O of PEP approaches Mn^{2+} from the sixth vertex defining an octahedral coordination sphere of the metal. However, the distance between Mn^{2+} and this carboxylate O (3.1 Å) is much greater than the typical range for Mn^{2+}−O distances, i.e., 2.0−2.4 Å; hence, PEP is not a metal ligand (Figure 3). The distance between Mn^{2+} and Oϵ1 of D302 is also long (3.2 Å). Thus, in contrast to the typical octahedral and tetrahedral coordinations, Mn^{2+} is coordinated by only five ligands in the E24Q DAHPS−Mn−PEP complex.

The conformation of PEP bound in the active site clearly deviates from its typical planar geometry (Figure 3). The molecule is rotated ~30° around the bond between C1 and C2. The planarity of the carboxylate (C2, C1, and carboxylate O atoms) and of the enol groups (C1−C3 and a bridging phosphate O) is retained; however, the two planes are rotated by ~30° relative to each other. Refinement results in the same geometry of PEP whether or not the planarities of the carboxylate and enol groups of PEP are restrained.

PEP is bound in the active site of the E24Q DAHPS−Mn−PEP complex by multiple H-bonds involving both its phosphate and carboxylate groups (Figure 3 and Table 3). The phosphate group is tightly fixed with each of its O atoms participating in at least two interactions with A164, R165, K186, or R234 or with water molecules. One of the carboxylate oxygen atoms, O1, interacts with Nη2 of R92, Nζ of K97, and water molecule Wa that also serves as a Mn^{2+} ligand, while the other, O2′, is coordinated by Nη1 of R92, Nζ of K186, and water Wb. H268 is located on the same side of the PEP carboxylate group as Mn^{2+}. The distance between Nϵ2 of H268 and the O atom of the PEP carboxylate is 3.4 Å, too long for a H-bond. The imidazole ring of H268 and the plane of the PEP carboxylate form a dihedral angle of ~45°; the closest approach between these planes is 2.8 Å.

Table 3: Polar Interactions Involved in PEP and PGL Coordination in E24Q DAHPS−Mn−PEP, DAHPS−Mn−PGL (*3*), and *A.a.* KDOPS−Cd−PEP (*16*) Complexes[a]

	E24Q DAHPS−Mn−PEP	DAHPS−Mn−PGL	KDOPS−Cd−PEP
O1	R92−Nη2 (2.85)	R92−Nη2 (2.98)	K41−Nζ (2.71)
	K97−Nζ (2.75)	K97−Nζ (2.84)	K46−Nζ (2.86)
	Wa (2.91)	Wa (2.87)	
	Mn^{2+} (3.11)	Mn^{2+} (2.40)	Cd^{2+} (4.12)
			S43−Oγ (3.15)
O2′	R92−Nη1 (3.06)	R92−Nη1 (2.93)	
	K186−Nζ (3.03)	K186−Nζ (3.34)	K124−Nζ (2.90)
	Wb (2.68)	Wb (2.57)	Q99−Oϵ1 (2.96)
O2	K186−Nζ (2.88)	K186−Nζ (2.64)	K124−Nζ (2.90)
	Wf (3.43)	Wf (3.08)	Wf (3.34)
O1P	A164−N (2.88)	A164−N (2.84)	A102−N (2.85)
	Wc (2.85)	Wc (3.03)	Wc (2.84)
	Wf (2.94)	Wf (3.14)	Wf (2.94)
		Wh (2.83)	
O2P	R165−Nη1 (2.80)	R165−Nη1 (3.02)	Wg (2.70)
	R234−Nη2 (3.24)	R234−Nη2 (3.41)	R154−Nη2 (2.81)
	Wd (2.71)	Wd (2.59)	
	We (3.18)		We (2.82)
O3P	K186−Nζ (2.94)	K186−Nζ (2.89)	K124−Nζ (2.82)
	R234−Nϵ (2.71)	R234−Nϵ (2.76)	R154−Nϵ (2.84)

[a] Distances in parentheses are in angstroms. Atoms are named according to the PDB convention for PEP (O1 and O2′ are carboxylate O atoms; O2 is a bridging phosphate O; O1P−O3P are three other phosphate O atoms). The distance between O1 of PEP and Cd^{2+} of the *A.a.* KDOPS−Cd−PEP complex is listed, although this interaction is negligible.

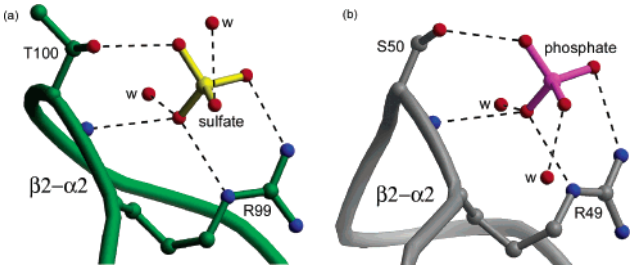

FIGURE 4: Similar binding sites of the E4P or A5P phosphate in DAHPS from *E. coli* and KDOPS from *A. aeolicus* formed by the residues of their $\beta 2-\alpha 2$ loops. (a) A sulfate ion from the crystallization medium is coordinated at the binding site of the E4P phosphate in the E24Q DAHPS−Mn−PEP complex by R99 and T100. Water molecules are denoted with the letter w. H-Bonds are shown as black dashed lines. (b) A phosphate ion from the crystallization medium is coordinated at the binding site of the A5P phosphate in the *A.a.* KDOPS−Cd−PEP complex by R49 and S50 (*16*).

Numerous water molecules are observed in the vicinity of the active site; most of them fill an opening of the channel at the C-end of the $(\beta/\alpha)_8$ barrel. Seven waters are located within contact distance of PEP. Two of these, Wa and Wb, form H-bonds with the carboxylate of PEP, and four others, Wc−Wf, participate in the coordination of the PEP phosphate; the remaining water molecule is 3.6 Å from the C3 atom of PEP (Figure 3 and Table 3). With the exception of We in subunit C, all seven water molecules are observed in all four subunits of the enzyme located in the asymmetric unit. The distance between C2 of PEP, which ultimately receives a hydroxyl group from water in the enzymatic reaction, and the closest water molecule, Wf, is 3.0 Å. Wf approaches C2 from the *re* face of PEP. The distances between C2 and the other surrounding water molecules are between 3.6 (Wa) and 5.1 Å (Wc).

As observed in the wild-type complexes, a sulfate anion from the crystallization medium is bound at the opening of the active site channel above PEP in the E24Q complex. The C3 atom of PEP, which forms a bond with C1 of E4P in the enzymatic reaction, is the PEP atom closest to the bound sulfate; the distance between C3 and S is 8.7 Å. The twist of the PEP plane orients its enol group so that the sulfate approaches it from its *si* side in accordance with the demonstrated stereochemistry of the reaction. The sulfate is coordinated by the side chain of R99 and by the peptide N and Oγ1 of T100 located at the bend of the $\beta 2-\alpha 2$ loop (Figure 4a). The higher resolution of the E24Q crystal permits several corrections in the coordination sphere of the bound sulfate. First, the side chain of R99 is not in a typical rotamer conformation; this enables both Nϵ and Nη2 to form contacts with different sulfate O atoms. In addition, two water molecules that participate in the sulfate coordination are now visible.

Although, as already mentioned, not all of the wild-type DAHPS−Mn−PEP structure is well-defined in the electron density, the active site is sufficiently resolved in three of the subunits to reveal a close correspondence with the active site of the E24Q enzyme, including the PEP twist and some of the bound water molecules.

DISCUSSION

The most significant feature of the active site of the E24Q DAHPS−Mn−PEP complex is the unusual geometry of the bound substrate. PEP is bound in an extended, twisted conformation with its enol and carboxylate planes forming a dihedral angle of ~30°; this we term the twist of the carboxylate group (Figure 3). In PEP in solution, the dihedral angle between the enol and carboxylate groups is ~0° because the molecule is stabilized by conjugation of their π-orbitals. This stabilization energy depends on the ionization state of PEP with the highest estimated value of ~6.5 kcal/mol in PEP^{1-} (*13*). The relative turn of carboxylate and enol planes by 30° is estimated to require ~3.5 kcal/mol in PEP^{2-} but has very low energy cost in both PEP^{1-} and PEP^{3-}. In DAHPS, PEP is coordinated by six Arg and Lys side chains and is inferred to be in its trianionic form. Thus, the enzyme appears to select a twisted conformation of PEP without the need to provide significant energetic assistance.

The phosphate of bound PEP is tightly anchored by eleven polar contacts with the N of A164, Nη1 of R165, Nζ of K186, Nϵ and Nη2 of R234, and the O atoms of waters Wc−Wf that surround it (Figure 3 and Table 3). On the other hand, Nη1 and Nη2 of R92, Nζ of K97, and Nζ of K186 that interact with the carboxylate of PEP are located approximately in its plane. It appears that the carboxylate of PEP rotates under the influence of Wb, which is positioned on the *re* side of PEP and pulls O2′ of the carboxylate due to a H-bond, and of Wa, which is located on the *si* side and attract O1 of the carboxylate. The interaction with Wb and Wa would force the carboxylate to rotate by more than 30°, but the rotation is balanced by the compensating influence of K97 and K186 so that the carboxylate O atoms are located within H-bonding distance of waters Wa and Wb as well as of the Nζ atoms of both K97 and K186 (Figure 3b).

Comparison with the Active Sites of DAHPS−Mn−PGL and DAHPS−Pb−PEP Complexes. The structure of the DAHPS−Mn−PGL structure determined at 2.0 Å resolution (*3*) shows a similar but smaller twist of phosphoglycolate bound in the active site. PGL is a structural analogue of PEP whose lack of an enol group enables free rotation of its carboxylate around the C1−C2 bond. PGL binds in a mode similar to that of PEP in the E24Q DAHPS−Mn−PEP complex but with some rearrangement of coordination (Figure 5a and Table 3). Superposition of the active site residues places the P atoms of PGL and PEP within 0.1 Å of each other; however, the orientation of the phosphate differs slightly. In contrast to PEP, the carboxylate O of PGL is a ligand of Mn^{2+}, which is located only 2.4 Å away. Besides the seven waters in the vicinity of PEP, the active site of the DAHPS−Mn−PGL complex contains an extra water molecule, Wh, H-bonded to a phosphate O of PGL. This water would not be able to be bound in the presence of PEP due to steric conflict with C3 that is absent in PGL. Consequently, We moves toward Wh, engaging it in an H-bond and abandoning a rather distant H-bond with the phosphate. The carboxylate of PGL is twisted in the same direction as the carboxylate of PEP, but the dihedral angle between the carboxylate plane and the plane defined by C1, C2, and the bridging phosphate O is only ~15° compared to an angle of 30° for PEP. The dihedral angle is smaller because the entire PGL molecule, which is anchored by its phosphate, rotates closer to Mn^{2+}, thereby decreasing the magnitude of the carboxylate twist. It is unclear why PEP does not have the same conformation as PGL because the closer interaction with Mn^{2+} should be advantageous

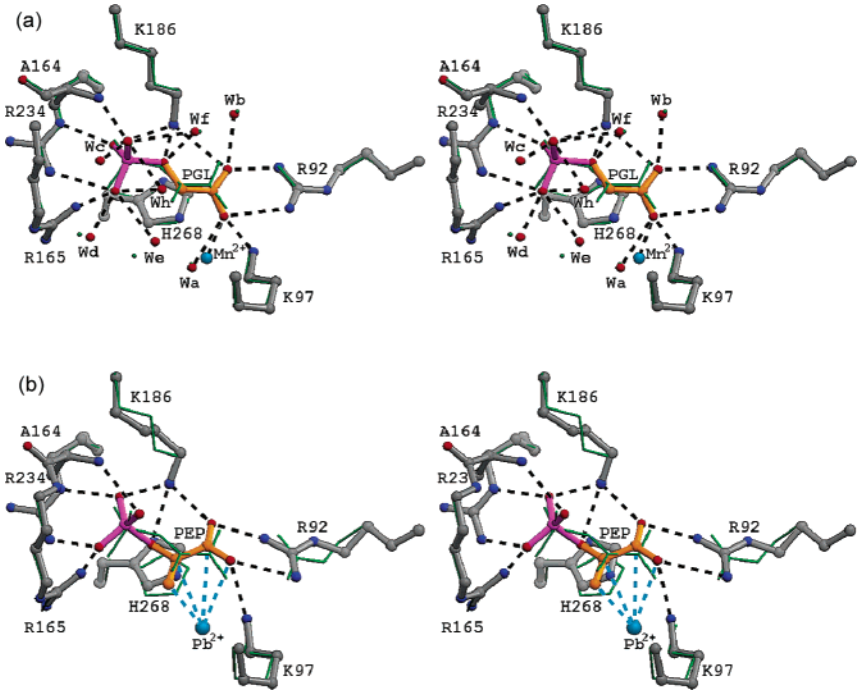

FIGURE 5: (a) Stereoview of the PGL-binding site in the DAHPS−Mn−PGL complex (*3*). The carboxylate O of PGL is a ligand of Mn^{2+} located 2.4 Å from it. Water molecules Wa−Wf are also present in the E24Q DAHPS−Mn−PEP complex; the counterpart of Wh is not seen in E24Q. The superimposed PEP-binding site of E24Q (Figure 3) is shown in green. H-Bonds are shown as black dashed lines. (b) PEP-binding site in the DAHPS−Pb−PEP complex (*2*). Pb^{2+} interacts with the conjugated π-system of PEP, preserving its planar geometry; the distances from Pb^{2+} to four atoms of PEP indicated by the dashed light blue lines are 3.6−3.9 Å.

considering that the other contacts would be nearly unaffected.

The DAHPS−Pb−PEP complex has a different type of interaction between the metal cation and PEP; this is probably responsible for its poor catalytic efficiency (*2*). The general position of PEP in the active site of the DAHPS−Pb−PEP complex (Figure 5b) is similar to that in PEP in the E24Q DAHPS−Mn−PEP complex and PGL in the DAHPS−Mn−PGL complex. The interactions of PEP with the residues of the enzyme are also similar (a wrong side chain rotamer was originally assigned to R234 because of a low resolution of 2.6 Å). This low resolution also precluded visualization of water molecules in the electron density of the DAHPS−Pb−PEP complex, but they probably occupy the same positions as observed in the E24Q DAHPS−Mn−PEP complex since the organization of the two active sites is similar. Although the fine details are obscured due to the low resolution, bound PEP appears to retain a planar geometry and is oriented so that four of the six atoms forming a plane, namely, C1−C3 and O1 of the carboxylate, approach Pb^{2+} at similar distances of 3.6−3.9 Å. This type of Pb^{2+} coordination was described for its complexes with organic compounds that possess a π-electron system such as crotonic acid (*14*). It is achieved due to the ability of the lone pair of $6s^2$ electrons of Pb^{2+} to develop p character (*15*). When this orbital conjugates with π-orbitals of a hemidirectionally coordinated organic ligand, Pb^{2+} lies near the perpendicular to the center of the plane containing the π-system, ~3.6 Å from that plane. We suggested that the planar structure of PEP is stabilized due to the conjugation of its π-orbitals with the $6s^2$ electron orbital of Pb^{2+} that has p character. This interaction changes the reactivity of PEP, making Pb^{2+} a poor metal activator.

PEP Binding in Other Enzymes. Entries in the Protein Data Bank for structures that contain bound PEP include the metal-dependent 2-keto-D-*manno*-2-octulosonate-8-phosphate synthase (KDOPS) from the hyperthermophilic bacterium *Aquiflex aeolicus* (*A.a.*) [several complexes at 1.85−1.94 Å resolution (*16*, *17*)], the metal-independent KDOPS from *E. coli* [2.8 Å (*18*)], yeast enolase [1.8 Å (*19*) and 2.0 Å (*20*)], and human PEP carboxykinase [2.0 Å (*21*)]. Of these, KDOPS is the only enzyme that is mechanistically and structurally similar to DAHPS. It catalyzes the analogous condensation of PEP and arabinose 5-phosphate (A5P) with the formation of 2-keto-D-*manno*-2-octulosonate 8-phosphate (KDOP). DAHPS is able to use A5P as a substrate, albeit poorly, while KDOPS is unable to utilize E4P, which is one carbon shorter than A5P (*22*). Both reactions are stereospecific with the *si* face of C3 of PEP attacking the *re* face of the aldehyde of E4P or A5P (*23*−*25*), and both involve the release of the phosphate of PEP by cleavage of the C−O rather than the O−P bond. The two other enzymes known to catalyze C−O cleavage, namely, 5-enolpyruvylshikimate-3-phosphate synthase (EPSPS) and UDP-*N*-acetylglucosamine enolpyruvyltransferase (MurA), are structurally and mechanistically similar to each other but differ significantly from DAHPS and KDOPS. In the reactions catalyzed by EPSPS and MurA, the intact enolpyruvyl group of PEP is transferred to the COH group of the second substrate, shikimate 3-phosphate and UDP-*N*-acetylglucosamine, respectively. High-resolution structures have been determined for several complexes of both EPSPS (*26*) and MurA (*27*, *28*), but none of these complexes contain PEP. The structures of PEP-bound complexes of the two enzymes that do not employ the cleavage of the C−O bond of PEP, namely, enolase and PEP carboxykinase, have been determined. Enolase catalyzes the addition of water to PEP to form 2-phospho-D-glycerate (2-PGA), while PEP carboxykinase catalyzes the carboxylation of PEP to oxaloacetate with the

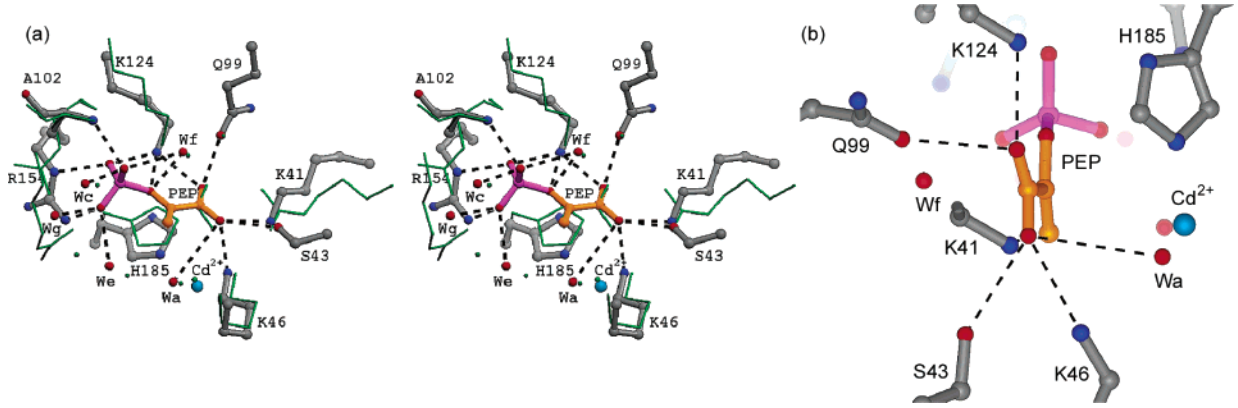

FIGURE 6: PEP-binding site of the metal-dependent KDOPS from *A. aeolicus*. The relative twist of its carboxylate and enol planes is ~10°. PEP-coordinating interactions (Table 3) are shown as black dashed lines. (a) A stereoview of the superimposed PEP-binding site of the E24Q DAHPS−Mn−PEP (Figure 3) is shown in green. (b) Interactions of the carboxylate group of PEP. The H-bond of the carboxylate O of PEP with S43 and the absence of its interactions with Wa and Cd^{2+} are responsible for the smaller twist. Wa and Wf are potential candidates for an attack at C2 of PEP in the enzymatic reaction.

release of phosphate from PEP by the cleavage of the O−P bond.

Prior to the availability of the three-dimensional structures of the enzymes, a theoretical analysis of PEP reactivity in the DAHPS, KDOPS, and EPSPS reactions was carried out by applying the hard−soft acid−base theory (*13*). The PEP conformations were predicted in these reactions on the basis of the hypothesis that the reactivity of PEP is controlled by the relative rotation of its carboxylate and enol groups. This twist and the ionization state of bound PEP define the charge and highest occupied molecular density at C3 and control whether C3 serves as a soft or hard base in the reaction. In the DAHPS and KDOPS reactions where C3 behaves as a soft basic atom, the twist of the PEP plane was predicted to be ~70° if the substrate binds as PEP^{2-} or ~90° if it binds as PEP^{3-}. In the EPSPS reaction, in which C3 is a hard base because it is protonated, PEP was predicted to bind in the dianionic form with its plane twisted by 30°. Our observations support the idea that a deformation of the planar structure of PEP is an important factor in DAHPS catalysis. Although the dihedral angle of 30° in PEP in the E24Q DAHPS−Mn−PEP complex differs from the predicted value of 90°, the twist may be altered when the enzymatic reaction proceeds upon the binding of the second substrate, E4P.

A different type of distortion of PEP geometry was described for the complexes of *A.a.* KDOPS with PEP (1.94 Å resolution), Cd^{2+} and PEP (1.9 Å), Cd^{2+}, PEP, and A5P (1.85 Å), Cd^{2+}, PEP, and E4P (1.9 Å), and Cd^{2+}, PEP, and ribose 5-phosphate (1.9 Å) (*16*, *17*). In all of these complexes, five of six atoms that define a plane in the unbound PEP, namely, C1, C2, O1, and O2 of the carboxylate and a bridging phosphate O, still reside in this plane. However, C3 bulges out of the *si* face of the plane by ~12° or 0.3 Å. This deviation from planarity was explained by the effect of the active site environment that prepares C2 of PEP for a conversion from sp^2 to sp^3 hybridization that occurs in the reaction intermediate.

The organization of the *A.a.* KDOPS active site has much in common with DAHPS, and the orientation and coordination of PEP in the two enzymes are similar (Figure 6 and Table 3). The superposition of the PEP molecules bound to *A.a.* KDOPS and the E24Q DAHPS using C1, C2, and five phosphate atoms places the corresponding coordinating residues in a very close position (Figure 6a). Interactions of the PEP phosphate with A102, K124, R154, Wc, We, and Wf in *A.a.* KDOPS are very similar to its contacts with A164, K186, R234, Wc, We, and Wf in DAHPS. Two differences in the phosphate coordination are related to the presence of F103 in *A.a.* KDOPS in place of R165 in DAHPS. The aromatic ring of F103 is turned aside, and the water, Wg, which is not present in DAHPS, is located near the position occupied by Nη2 of R165 in DAHPS, which coordinates the same phosphate O. Wd, which forms a H-bond with O2P of PEP phosphate and was also stabilized by R165 in DAHPS, is absent in *A.a.* KDOPS. The resulting orientation of the PEP phosphate in *A.a.* KDOPS is nearly identical to that in DAHPS.

The coordination of the PEP carboxylate in *A.a.* KDOPS and in DAHPS has more differences. Its interactions with K46 and K124 in *A.a.* KDOPS and K97 and K186 in DAHPS are similar. R92 in DAHPS is substituted in *A.a.* KDOPS with K41, whose Nζ interacts with O1 of the PEP carboxylate and is also located approximately in the carboxylate plane. Wb, which interacts with O2 of the PEP carboxylate in DAHPS, is replaced in *A.a.* KDOPS with Oγ1 of Q99 located at the same position. This Oϵ1 forms a similar H-bond with O2 and should be able to provide the same driving force for the rotation of the carboxylate that Wb does in DAHPS. However, in *A.a.* KDOPS, its impact is compensated by an H-bond between O1 of the carboxylate and Oγ of S43 positioned on the same side of the carboxylate plane as is Oϵ1 of Q99, which is not present in DAHPS. In contrast to DAHPS, O1 does not interact with Wa and Cd^{2+} located on the other side of the carboxylate plane (distances of 3.6 and 4.1 Å, respectively). O1 therefore lacks the second factor responsible for the carboxylate twist. When the 30° twist of the PEP carboxylate is modeled, a slight adjustment of PEP would bring the carboxylate O atoms to the position where they interact with Oϵ1 of Q99, Wa, and Cd^{2+} as observed in DAHPS while the H-bond with Oγ of S43 would be lost.

The difference in the distortion of the PEP geometry in the similar binding sites of DAHPS and of *A.a.* KDOPS presents something of an enigma. No deformation of either the enol or the carboxylate planes is observed in PEP in the E24Q DAHPS−Mn−PEP complex. We cannot identify a

factor that causes C3 of PEP to bulge out of the enol plane in *A.a.* KDOPS but is absent in DAHPS. Calculation of the electron density of the PEP-containing complexes of *A.a.* KDOPS from the coordinates and structure factors deposited in the PDB database shows that PEP is well-defined in the density and deviates noticeably from planarity. However, PEP can be satisfactorily built into the density by moving C3 out of the enol plane as was described previously (*16*) and/or by twisting its carboxylate group by ~10°. Although the resolution of the *A.a.* KDOPS structures is high, it is not sufficient for distinguishing clearly between alternative geometries of the bound PEP. We suggest that the conformation of PEP bound in *A.a.* KDOPS deviates from planarity due to the 10° relative rotation of its enol and carboxylate planes similar to the 30° rotation observed in DAHPS. The larger magnitude of the PEP twist in DAHPS facilitates its identification. The smaller twist in *A.a.* KDOPS might be related to the fact that the structure of this hyperthermophilic enzyme was determined at low temperatures where it has no detectable activity. However, we cannot completely dismiss the possibility that DAHPS and *A.a.* KDOPS modify the conformation of the bound PEP in different ways. The structure of the PEP-containing complex of metal-independent KDOPS from *E. coli* was determined at 2.8 Å resolution (*18*), a resolution that is too low for observation of the details of PEP conformation.

Neither of the two enzymes that catalyze reactions involving the breaking of the C−O bond of PEP in the release of phosphate demonstrates significant relative rotations of the enol and carboxylate groups of the bound PEP. In the 2.0 Å resolution structure of PEP carboxykinase with bound PEP, Mn^{2+}, and Na^{+} (*21*), the observed substrate twist is ~9° while the deformation of the enol and carboxylate planes is ~5° and ~3°, respectively. One of the two independently reported structures of the PEP−enolase complex contains an equilibrium mix of PEP and 2-PGA and two Mg^{2+} atoms at both active sites of the enolase dimer [determined to 1.8 Å resolution (*19*)], while the second structure is asymmetric with PEP and Mg^{2+} bound to one enzyme subunit and 2-PGA, Mg^{2+}, and Li^{+} to the other [2.0 Å resolution (*20*)]. No significant twist of enol and carboxylate is observed in either complex, but the planarities of the enol and carboxylate groups of PEP are distorted by 8° and 5°, respectively, in the symmetric enolase structure and by 12° and 6°, respectively, in the asymmetric one. The deformations of the three planes recognized in PEP (enol, carboxylate, and a common plane that includes both groups) in both PEP carboxykinase and enolase appear to be within the appropriate limits for resolution-related errors and do not indicate any major distortion of the typical planar geometry of PEP. Thus, DAHPS is the only enzyme that has been shown to induce a large twist of the carboxylate group of the bound PEP, suggesting that this is a critical factor in the mechanism of enzymatic reactions involving C3 of PEP.

E4P Binding and the DAHPS Catalytic Mechanism. The E24Q DAHPS−Mn−PEP structure contains a sulfate bound at the opening of the active site channel that marks the binding site of the E4P phosphate. Similarly, the binding site of the A5P phosphate is occupied by a phosphate anion present in the crystallization media in the complexes of *A.a.* KDOPS that do not contain A5P or its analogues (*16*). In both DAHPS and KDOPS, the binding site of the E4P or A5P phosphate is located on the *si* side of the PEP enol group so that the aldehyde group of E4P or A5P is able to approach C3 of PEP from only the *si* face, in agreement with the established stereochemistry of the reactions. A very similar coordination of sulfate and phosphate in DAHPS and KDOPS is provided by unusual rotamers of Arg (R99 in DAHPS or R49 in *A.a.* KDOPS) and by the following Thr (in DAHPS) or Ser (in *A.a.* KDOPS) located on the bend of the $\beta 2-\alpha 2$ loop (Figure 4). Although E4P is one carbon shorter than A5P, the 8.7 Å distance between C3 of PEP and the S of the sulfate in DAHPS is close to the distance (9.0 Å) between C3 of PEP and the P of the A5P phosphate or the phosphate anion bound in its place in *A.a.* KDOPS.

When E4P in the extended conformation is modeled into the DAHPS structure with its phosphate anchored at the sulfate binding site, C1 of E4P approaches within 2.4 Å of C3 of PEP. This supports the hypothesis that the condensation proceeds through a linear intermediate with a water molecule attacking C2 of PEP (*29*) rather than through the cyclic intermediate with the C3-OH group of E4P or A5P attacking C2 of PEP. Two water molecules, Wf and Wa, located 3.0 and 3.6 Å, respectively, from C2 of PEP, are the potential candidates for the attack. Analogous water molecules are present in *A.a.* KDOPS, 3.2 and 3.5 Å from C2 of the bound PEP. Duewel et al. (*16*) proposed a nucleophilic attack on C2 by the hydroxide ion that originates from Wa. This water is a metal ligand and also forms an H-bond with Nζ of K97 in DAHPS or K46 in *A.a.* KDOPS. These interactions are expected to lower the pK_a of Wa, facilitating its ionization. However, Wa is positioned on the same side of the PEP enol as is the aldehyde of E4P or A5P. Therefore, the reaction initialized by the attack of OH^{-} originating from Wa on C2 of PEP would represent an unusual *syn* addition of water and A5P to the *si* side of PEP.

In contrast, Wf is more appropriately located on the opposite side of the enol plane of PEP from the aldehyde of E4P or A5P and is closer to C2 of PEP than to Wa. However, in both enzymes, Wf is involved in three H-bonds that are unlikely to facilitate its transformation into OH^{-} by the abduction of its proton. In DAHPS, Wf participates in H-bonds with Oϵ1 of E143, Wb, and O of the PEP phosphate. In *A.a.* KDOPS, Wf interacts with Oδ2 of D81, Oϵ1 of Q99, and O of the PEP phosphate. The proton transfer chain consisting of D81 and H83 could potentially be involved in the abduction of H^{+} from Wf in *A.a.* KDOPS (*16*), but such a chain is not present in DAHPS. Thus, at present it is impossible to determine whether Wa or Wf is involved in the attack at C2 of PEP in the reaction. Work on the structures of DAHPS complexes containing E4P and its analogues now under way in our laboratory should clarify the mode of E4P binding and reveal the catalytic mechanism of DAHPS.

ACKNOWLEDGMENT

Diffraction data were collected at the National Synchrotron Light Source (NSLS) at Brookhaven National Laboratory (Upton, NY). We thank Craig Ogata and the staff of beamline X4A for assistance and advice. We thank Gregory Dick and Chang Zhao for preparing and characterizing the mutant DAHPSs.

REFERENCES

1. Bentley, R. (1990) *Mol. Biol. 25*, 307−384.
2. Shumilin, I. A., Kretsinger, R. H., and Bauerle, R. (1999) *Struct. Folding Des. 7*, 865−875.
3. Wagner, T., Shumilin, I. A., Bauerle, R., and Kretsinger, R. H. (2000) *J. Mol. Biol. 301*, 389−399.
4. Shumilin, I. A., Zhao, C., Bauerle, R., and Kretsinger, R. H. (2002) *J. Mol. Biol. 320*, 1147−1156.
5. Shumilin, I. A., Kretsinger, R. H., and Bauerle R. (1996) *Proteins 24*, 404−406.
6. Otwinowski, Z., and Minor, W. (1997) *Methods Enzymol. 276*, 307−326.
7. Collaborative Computational Project Number 4 (1994) *Acta Crystallogr. D50*, 760−763.
8. Brünger, A. T., Adams, P. D., Clore, G. M., DeLano, W. L., Gros, P., Grosse-Kunstleve, R. W., Jiang, J. S., Kuszewski, J., Nilges, M., Pannu, N. S., Read, R. J., Rice, L. M., Simonson, T., and Warren, G. L. (1998) *Acta Crystallogr. D54*, 905−921.
9. Jones, T. A., Zou, J. Y., Cowan, S. W., and Kjeldgaard, M. (1991) *Acta Crystallogr. A47*, 110−119.
10. Lamzin, V. S., and Wilson, K. S. (1997) *Methods Enzymol.* 277, 269−305.
11. Laskowski, R. A., MacArthur, M. W., Moss, D. S., and Thornton, J. M. (1993) *J. Appl. Crystallogr. 26*, 283−291.
12. Stephens, C. M., and Bauerle, R. (1991) *J. Biol. Chem. 266*, 20810−20817.
13. Li, Y., and Evans, J. N. (1996) *Proc. Natl. Acad. Sci. U.S.A. 93*, 4612−4616.
14. Clegg, W., Little, I. R., and Straughan, B. P. (1986) *Acta Crystallogr. C42*, 1319−1322.
15. Shimoni-Livni, L., Glusker, J. P., and Bock, C. W. (1998) *Inorg. Chem. 37*, 1853−1867.
16. Duewel, H. S., Radaev, S., Wang, J., Woodard, R. W., and Gatti, D. L. (2001) *J. Biol. Chem. 276*, 8393−8402.
17. Wang, J., Duewel, H. S., Woodard, R. W., and Gatti, D. L. (2001) *Biochemistry 40*, 15676−15683.
18. Asojo, O., Friedman, J., Adir, N., Belakhov, V., Shoham, Y., and Baasov, T. (2001) *Biochemistry 40*, 6326−6334.
19. Larsen, T. M., Wedekind, J. E., Rayment, I., and Reed, G. H. (1996) *Biochemistry 35*, 4349−4358.
20. Zhang, E., Brewer, J. M., Minor, W., Carreira, L. A., and Lebioda, L. (1997) *Biochemistry 36*, 12526−12534.
21. Dunten, P., Belunis, C., Crowther, R., Hollfelder, K., Kammlott, U., Levin, W., Michel, H., Ramsey, G. B., Swain, A., Weber, D., and Wertheimer, S. J. (2002) *J. Mol. Biol. 316*, 257−264.
22. Sheflyan, G. Y., Howe, D. L., Wilson, T. L., and Woodard, R. W. (1998) *J. Am. Chem. Soc. 120*, 11027−11032.
23. Floss, H. G., Onderka, D. K., and Carroll, M. (1972) *J. Biol. Chem. 247*, 736−744.
24. Kohen, A., Berkovich, R., Belakhov, V., and Baasov, T. (1993) *Bioorg. Med. Chem. Lett. 3*, 1577−1582.
25. Dotson, G. D., Nanjappan, P., Reily, M. D., and Woodard, R. W. (1993) *Biochemistry 32*, 12392−12397.
26. Schonbrunn, E., Eschenburg, S., Shuttleworth, W. A., Schloss, J. V., Amrhein, N., Evans, J. N., and Kabsch, W. (2001) *Proc. Natl. Acad. Sci. U.S.A. 98*, 1376−1380.
27. Eschenburg, S., and Schonbrunn, E. (2000) *Proteins 40*, 290−298.
28. Schonbrunn, E., Eschenburg, S., Luger, K., Kabsch, W., and Amrhein, N. (2000) *Proc. Natl. Acad. Sci. U.S.A. 97*, 6345−6349.
29. DeLeo, A. B., Dayan, J., and Sprinson, D. B. (1973) *J. Biol. Chem. 248*, 2344−2353.
30. Carson, M. (1997) *Methods Enzymol. 277*, 493−505.

BI027257P